water

MDPI

Article

Experimental Study of Influence of Karst Aquifer on the Law of Water Inrush in Tunnels

Weimin Yang [1,2], Zhongdong Fang [1,2], Xin Yang [1], Shaoshuai Shi [1,2,3,*], Jing Wang [1,2], Hao Wang [1], Lin Bu [1,2], Liping Li [1,2], Zongqing Zhou [1,2,3] and Xueqing Li [4]

1 Geotechnical and Structural Engineering Research Center, Shandong University, Jinan 250061, China; weimin.yang@sdu.edu.cn (W.Y.); 201613357@mail.sdu.edu.cn (Z.F.); sduyangxin@gmail.com (X.Y.); wjingsdu@163.com (J.W.); wanghao15@mail.sdu.edu.cn (H.W.); 201520363@mail.sdu.edu.cn (L.B.); yuliyangfan@163.com (L.L.); Zongqing.Zhou@sdu.edu.cn (Z.Z.)
2 School of Qilu Transportation, Shandong University, Jinan 250061, China
3 State Key Laboratory of Mining Disaster Prevention and Control, Shandong University of Science and Technology, Qingdao 266590, China
4 School of Software, Shandong University, Jinan 250101, China; xqli@sdu.edu.cn
* Correspondence: shishaoshuai@sdu.edu.cn

Received: 1 August 2018; Accepted: 5 September 2018; Published: 7 September 2018

check for updates

Abstract: Water inrush is a geological hazard often encountered in tunnel construction. In order to overcome problems encountered when using the existing water-inrush simulation model test, such as single function, low repetition utilization rate, and poor visibility, we developed a multi-type water-inrush model test system. Our test system can be a precursor to large-scale studies, handle multiple types, and perform serialization and visualization. We conducted cavity water-inrush simulation testing using this device, and studied the failure model of aquifuge rock. We reveal the evolution laws of water inrush from the cavity, including the initiation of fracture in the aquifuge rock, the formation of water-inrush channels, and the rupture of the aquifuge rock. By analyzing the seepage pressure changes at the monitoring points of the aquifuge rock, we divided the water-inrush process of the cave into a rack generation stage, a holing-through of fracture and forming of water-inrush channel stage, and a water-inrush stage. Test results show that the system is stable and reliable, only requiring a short test period, and can be used to guide large water-inrush testing and related projects.

Keywords: karst aquifer; water inrush; hydraulic; model test; evolution law

1. Introduction

Water inrush from tunnels is always a hot topic in the geotechnical engineering field. If the aquifuge structure is disturbed or exposed during tunnel construction, geological disasters, such as water inrush and mud gushing, are easily induced, often causing significant casualties and property loss. Therefore, in order to ensure the safety of tunnel construction, it is of important theoretical and practical significance to study deeply the mechanism of water inrush and mud gushing occurrence [1–6]. The geo-mechanical model test is intuitive and comprehensive, the test conditions can be controlled and changed, and the model avoids mathematical and mechanical problems. So, the test method is an important process used to study rock-mechanics problems encountered by underground engineering. Researchers completed many experimental studies on the mechanism of water-inrush disaster in tunnels [7–9].

Sterpi and Cividini discussed the behavior up to failure of shallow underground openings on the basis of small-scale model laboratory tests and finite element simulation. The experimental results were obtained from two-dimensional (2D; plane strain) and three-dimensional (3D) tunnel models tested under standard gravity conditions. The comparison between experimental and numerical results led to conclusions about the influence of strain localization on the overall behavior of shallow tunnels and on the stability of their headings [10]. Li et al. developed a fluid–solid coupling test system for subsea tunnels based on the Qingdao Jiaozhou bay subsea tunnel, and studied the failure regularity of the surrounding rock during the construction process of the submarine tunnel [11]. Liang et al. analyzed the change laws of stress, displacement, and water pressure using physical simulation experiments of water inrush during tunnel excavation. They divided the whole water-inrush process into two periods: accumulation and instability. They established the criteria for water inrush based on the test results, actual engineering cases, and cusp catastrophe theory [12]. Jiang et al. researched and manufactured a 3D model test system that can be applied to simulate water-inrush geohazards. They carried out a series of large-scale geo-mechanical model tests based on the test system. Model test results demonstrated two main destruction characteristics on the tunnel face for water-inrush disaster: shear failure occurring at the center of the tunnel face, and osmotic instability occurring at the edge of tunnel face [13]. Wang et al. physically simulated the construction process of deeply buried diversion tunnels under high osmotic pressure, and studied the seepage and evolution law of the tunnel during the construction process of the background of the diversion tunnel project for the Jinping secondary hydropower station [14]. Pang et al. found that floor water inrush necessarily occurs when mining pressure leads to the extension and transfixion of a crack, and the sufficient condition for floor water inrush is that the confined water's expansionary stress in the normal direction and shear stress in the tangential direction must be larger than the internal stress in the crack [15]. Zhang et al. simulated the entire process of crack formation, concealed fault propagation, and evolution of a water-inrush channel with high-pressure water directly beneath the mine floor based on fluid–solid coupling mechanics and solid materials research. The results indicated that water channels are mainly caused by the connection between tectonic rock zones and coal floor cracks, which are the direct cause of water inrush [16].

Considering the abovementioned findings, a large model test must be real and intuitive, and simulate actual construction situations. However, the human, time, and material investment in large-scale model tests is too large. Because the current model test system is often designed for specific types of working conditions, the repetition rate is low and visibility is poor, and since the volume is large, filling the model is laborious. In this study, we developed a tunnel water-inrush simulation indoor test system in order to solve the problems experienced by the existing model test system. The system can simulate multiple types and multiple angles of water inrush, and enables the study of the variation in the stress field and seepage field in the process of water inrush. This model can be conveniently filled, only requires a short test period, and has a high repetition use rate and strong visibility. Then, to study characteristics of water inrush from different orientations, we performed a series of small-scale model tests. Finally, we analyzed the failure mode of aquifuge rock and the variation regularity of seepage pressure in the aquifuge rock. The experimental results provide data support and guidance for prediction of water-inrush disaster.

2. Experimental Apparatus

2.1. The Purpose of Developing the Test System

There are three kinds of water inrush divided by failure mode in karst areas: (1) non-geological defect-type water inrush, which is the broken water of the complete surrounding rock; (2) geological defect-type water inrush, such as fault, dissolved cavity, karst pipeline, and other water-containing tectonic water inrush; and (3) combined water inrush, which is the combination of the above two types [17].

Many scholars only study one of these water-inrush types, and thus, developed test systems can only be applied to specific engineering situations. As such, aiming at the problems of the current model test system, such as single function, low repetition utilization rate, and poor visibility, we developed a tunnel water-inrush simulation indoor test system, the main purposes of which are as follows:

(1) Precursor: The test system we developed has a short test cycle, saves manpower and material resources, and can be used for statistical test characteristics. Therefore, according to the working conditions, small-scale simulation tests can be carried out before conducting large-scale model tests. The later tests should be better improved by summarizing the relevant laws and combining numerical tests. Small model tests can be used as pilot tests for large model tests.
(2) Multiple types: The existing water inrush chamber test system was developed for particular working conditions; therefore, it cannot realize the simulation test of many types of water inrush. Our system was developed to simulate various types water inrush, such as cavity water inrush, water inrush from fault, and bursting water of the complete rock body.
(3) Serialization: This test system was designed as an extensible test system, and the inner diameter of the main box can be changed from 30 to 70 cm to accommodate different scale tests.
(4) Visualization: The main box of the test system is made of acrylic glass in order to improve viewing the test process.

2.2. Composition of the Test System

The simulation test system of tunnel water inrush consists of two parts: the main test system and the hydraulic loading system, as shown in Figure 1.

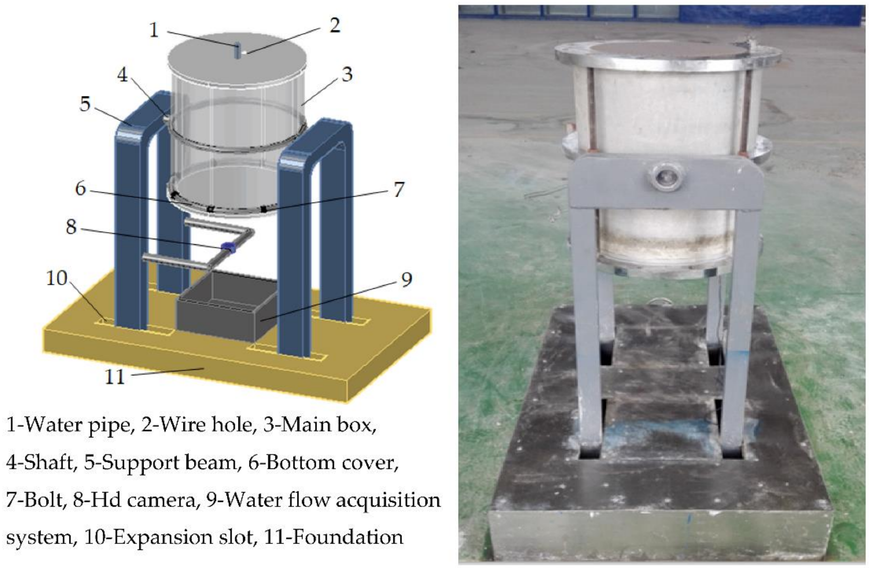

(**a**) (**b**)

Figure 1. Multi-type water-inrush test system. (**a**) Design drawing of master system; (**b**) picture of real product.

The main box is made of 2-cm-thick acrylic glass, which is the basic site of the test, and it has an inner diameter of 45 cm and a cylinder height of 50 cm. The system not only ensures the visual requirements of the test, but also the strength of the test model. The middle part is fitted with an annular steel rim with an inner diameter of 45.2 cm and outer diameter of 47.2 cm, connected with a bracket, allowing the box to rotate 360° around the rotating shaft and be fixed on the shaft, which solves the angle problem in water-inrush simulation testing. For example, in the karst cave simulation test, the main body in the hinge, 0°, 90°, and 180° correspond to the working conditions of the top, side, and bottom of the karst cave, respectively.

The difference between the seepage field and the stress field during the process of water inrush in different locations was compared by experiments. If a high-hydrostatic test is carried out inside the box, the steel rim ensures the strength of the box. The top and bottom are flange-connected. The top cover is equipped with a water pipe and the outlet hole in order to facilitate access to component lines. The bottom is a replaceable chassis, including an annular pallet and round-hole chassis; therefore, different types of chassis can be installed according to different types of tests. The annular pallet simulates and excavates the temporary surface, and completes the simulation test of the fractured rock body, simulation test of water inrush in karst cave, and simulation test of minimum safety thickness, etc. For a round-hole chassis, a variety of simulation tests, such as seepage instability and fault water inrush, can be carried out. Multi-type and repeated use are realized, and a statistic sample test can be carried out as the test period is short. The chassis types are shown in Figure 2.

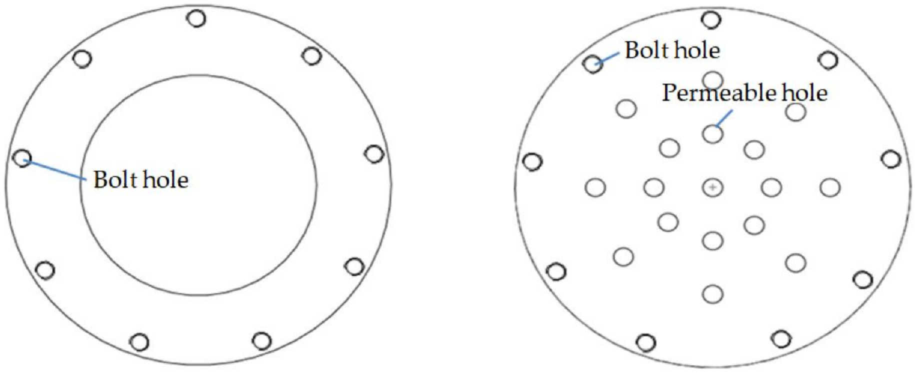

(**a**) (**b**)

Figure 2. The bottom form. (**a**) Annular tray; (**b**) circular-hole chassis.

The bracket system consists of a base and a bracket beam. The bracket is composed of two "∏" type bracket beams, and its main function is fixing and supporting the main box. The bracket has a hinge, which fixes the main box at any angle. A camera bracket is provided on the bracket beam, which can be fitted with a high-definition (HD) camera according to the test needs. For example, when the main box is in a vertical state (0°), a high-definition camera is added at the bottom to clearly observe the changes at the bottom of the model during the test. The pedestal has an expansion trough, and the support beam may move along the expansion trough. Thus, the disassembly and installation of the main box are convenient, and meet the requirements of different scale tests (boxes of different scales). A water-collecting device is arranged on the base to collect gushing water during the analysis test.

The hydraulic pressure loading system consists of a pressure-retaining pump and an air compressor. The pressure-retaining water pump has two modes: manual control of water pressure and micro-computer automatic control pump hydraulic pressure, which was self-developed by the Shandong University. The hydraulic control range of a single pump (without a connected air compressor and other correlative device to provide addition load pressure) is 0 to 6 MPa. Additionally, the pump water pressure information of the test process is exported through an ordinary external memorizer after the test, because the pressure-retaining water pump automatically records the changes in the water pump pressure without an external device. So, the water pump fully meets the test requirements. The air compressor provides additional power for the pressure-retaining pump to increase the maximum water pressure to 50 MPa. The hydraulic pressure loading system meets the needs of different types of tests with easy operation, a large controllable water pressure range, and a pressure-retaining function.

3. Test Materials and Methods

3.1. Test Materials

We selected fluid–solid coupling similar materials newly developed by Shandong University to simulate surrounding rock. The similar material uses cement and chlorinated paraffin as a cementing agent; uses sand, iron powder, and calcium carbonate as the aggregate; and silicone oil with the appropriate amount of mixing water as a regulator [18]. Basic components of the similar materials and fabrication specimens are shown in Figure 3. The materials used in the test are shown in Table 1. In the water-inrush simulation test, in addition to the basic mechanical parameter tests of similar materials, the water characteristics of similar materials must be tested. The specimens were immersed in water, and the compressive strength of specimens after immersion was changed from 0.45 MPa to 0.46 MPa and 0.42 MPa when soaked seven days and 28 days, respectively. It can be seen that the material was not obviously softened after being soaked, which satisfies the testing demand. Table 2 provides the basic mechanical parameters of the similar materials under the above ratio.

Figure 3. The similar material components and the specimen. (**a**) Basic composition of the material; (**b**) production of similar material specimen.

Table 1. Similar material proportion.

Sand	Calcium Carbonate	Iron Powder	White Cement	Silicone Oil	Chlorinated Paraffin
1	0.08	0.07	0.08	0.02	0.14

Table 2. Similar material physical and mechanical parameters.

Medium	Density (g/cm^3)	Compressive Strength (MPa)	Elasticity Modulus (MPa)	Poisson Ratio
Similar material	2.4	0.45	42.3	0.27

3.2. Method

This test was divided into three kinds of working conditions. The main box was rotated 0°, 90°, and 180° to simulate the water inrush of a vault cave, cave in front of the tunnel face, and cave at the bottom of the tunnel, respectively, as shown in Figure 4. We adopted the method of tamping and filling in the layer for this test. Firstly, the model body was filled under the vertical state of the main box (0°). The material was weighed in order to ensure the density of the model, and then, artificially tamped to the predetermined altitude. The main box with a certain angle of rotation was used according to the test requirement after the model body was stabilized.

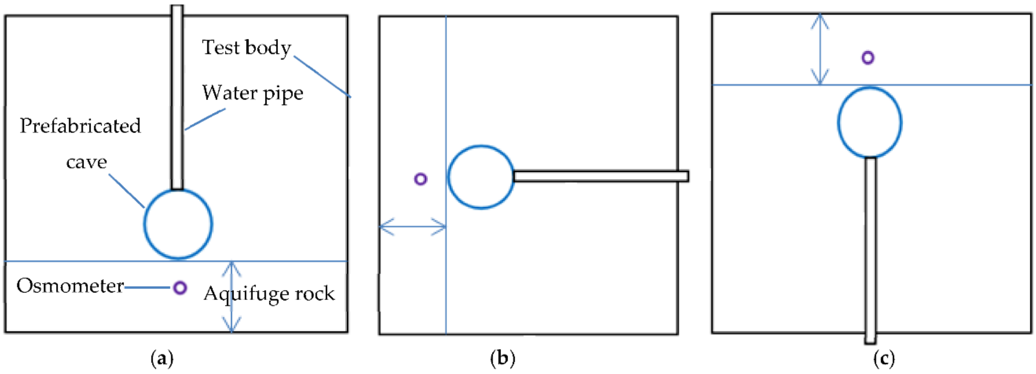

Figure 4. Picture of the indoor test. (**a**) The vault cavity; (**b**) the cavity in front of the tunnel face; (**c**) the cavity at the bottom of arch.

The thickness of the aquifuge rock was set to 4.2 cm based on the literature and testing the water-inrush thickness of the aquifuge rock body [19]. A spherical cavity with a diameter of 10 cm at the top of the aquifuge rock was precasted to simulate the cave, and a water pipe with an inner diameter of 1.5 cm was connected to the top of the cave. In the test, the water pipe was connected with the pressure-retaining pump, to recharge the dissolved cavity and simulate the pressure change in the karst cave, until the aquifuge rock body fractured and the karst-cave water inrush occurred. A miniature osmometer was planted in the aquifuge rock body to monitor the change in seepage pressure during the test process, because if the test scale is too small, too many embedded monitoring elements will affect the test results, and the main purpose of this test was to study the failure mode and macroscopic law of the aquifuge rock during the karst water inrush process.

To monitoring the filling of components, the position of the monitoring element was first positioned according to the design position after being reclaimed to the monitoring element. Secondly, the monitoring element was placed in the system after digging groove openings. Finally, similar materials were backfilled and tamped. The monitoring element line was drawn from the side wall.

For the hydraulic loading scheme, the pump was turned on during the test. The pressure was increased at the rate of 60 kPa/min after the water was filled with dissolved cavities. Pressure maintenance started when the pressure reached 0.3 MPa. After the pump maintained the pressure state for 10 min, the model body was continually stepped up at the original rate to 0.6 MPa and pressure was maintained for 10 min without significant changes, such as fracture, until water inrush occurred.

4. Results and Discussions

4.1. Failure Mode of the Aquifuge Rock

4.1.1. Water Inrush in the Vault Cavity

For the seepage stage before water inrush, the water pressure was increased at the rate of 60 kPa/min according to the hydraulic loading scheme. The seepage phenomenon occurred in the part of the aquifuge when the pressure reached 0.1 MPa, and the seepage phenomenon spread from the local area below the prefabricated dissolved cavity to the whole rock body with the increase in water pressure (Figure 5).

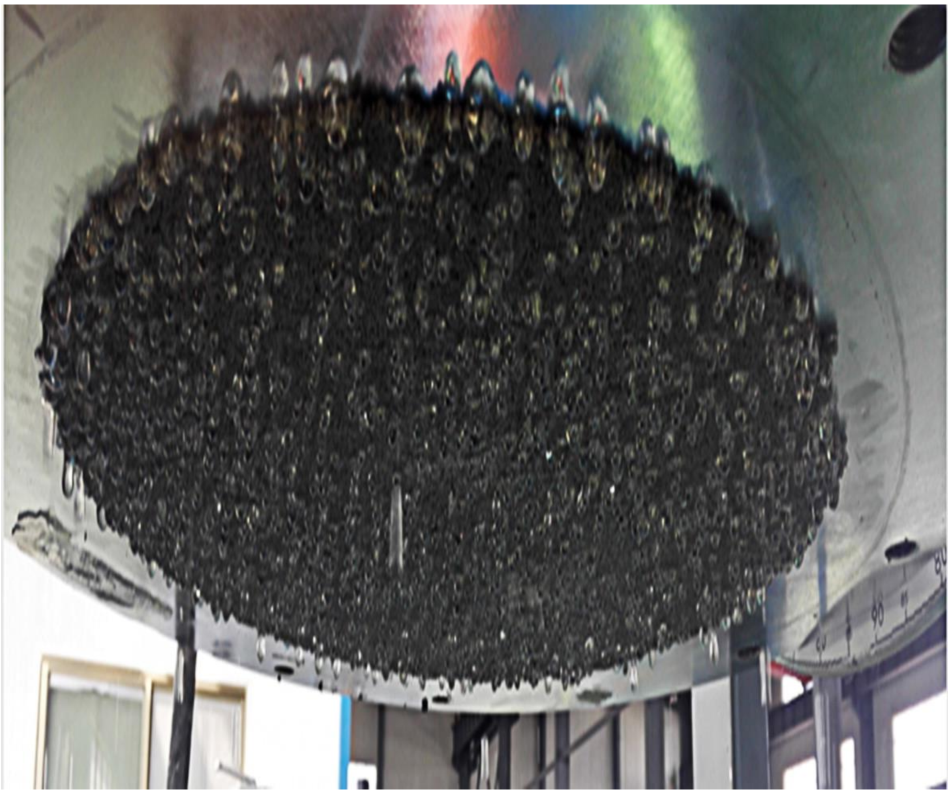

Figure 5. Water seepage stage in the vault cavity.

For the water-inrush stage, the speed of seepage accelerated with increasing hydraulic pressure. The local seepage of water was faster at the bottom when the hydrostatic pressure reached 0.3 MPa. The fracture of the bottom aquifuge rock broke after about five minutes of keeping the water pressure constant, as shown in Figure 6. The fracture of the bottom aquifuge rock extended from the middle to the boundary. The water inrush was mainly concentrated in the lower part of the prefabricated dissolved cavity after the fracture of the aquifuge rock occurred, and there was a crack of about 2 cm below the dissolved cavity, forming the main water inrush. It can be seen from the figure that there is a large flow which converges in the vicinity of the water inrush, and protrudes from the water outlet. There are three small cracks in the junction of the dissolved cavity and the aquifuge rock body, and a small stream of water flows out.

At the water-inrush stop stage, the water pump began releasing pressure after water inrush occurred, and when the pump returned to the natural water supply state, the pump was closed to stop the water supply. After water inrush occurred, the main water inrush was measured at about 2 cm, the thickness was about 0.8 cm, and the maximum width was about 0.1 cm.

Figure 6. Water-inrush stage in the vault cavity.

4.1.2. Water Inrush of Cavity in Front of the Tunnel Face

At the seepage stage before water inrush, hydraulic loading was carried out according to the hydraulic loading scheme. The lower part of the aquifuge (below the dissolution cavity) began demonstrating the seepage phenomenon when the water pressure reached 0.1 MPa. With increasing water pressure, the seepage area eventually covered the entire water body surface from bottom to top. However, we clearly observed that the upper area of the aquifuge rock was dripping when the surface of the aquifuge was covered by the water seepage. The lower area, especially under the prefabricated dissolution cavity where the seepage area began to appear, showed a pronounced flow of strands. We predicted that the region would become the weak area, that is, the drop or the water-inrush area, as shown in Figure 7.

For the water-inrush stage, we gradually increased the water pressure. When the water pressure reached 0.3 MPa, we controlled the water pump to enter the pressure-retaining state. The water seepage in the area below the aquifuge rock increased abnormally, and the femoral water seepage was connected into a piece, showing a local water-inrush trend. After the water pressure-retaining time was maintained for the designated time, there was no rupture in the aquifuge rock, and there was no abnormal change in the test phenomenon. Thus, we continued increasing the water pressure.

The water seepage in the lower part of the seepage area obviously increased when the water pressure reached 0.34 MPa, and the boundary between the lower seepage area and middle and upper water seepage area was obvious. Then, a micro-crack appeared below the dissolved cavity, which extended to the edge of the model body about 20° to the lower right. The crack expanded and extended to the upper left under the action of water pressure, but its elongation was obviously lower than the crack propagation speed. At the same time as the crack extended and expanded, there was an obvious uplift phenomenon at the bottom of the model and in the aquifuge near the crack.

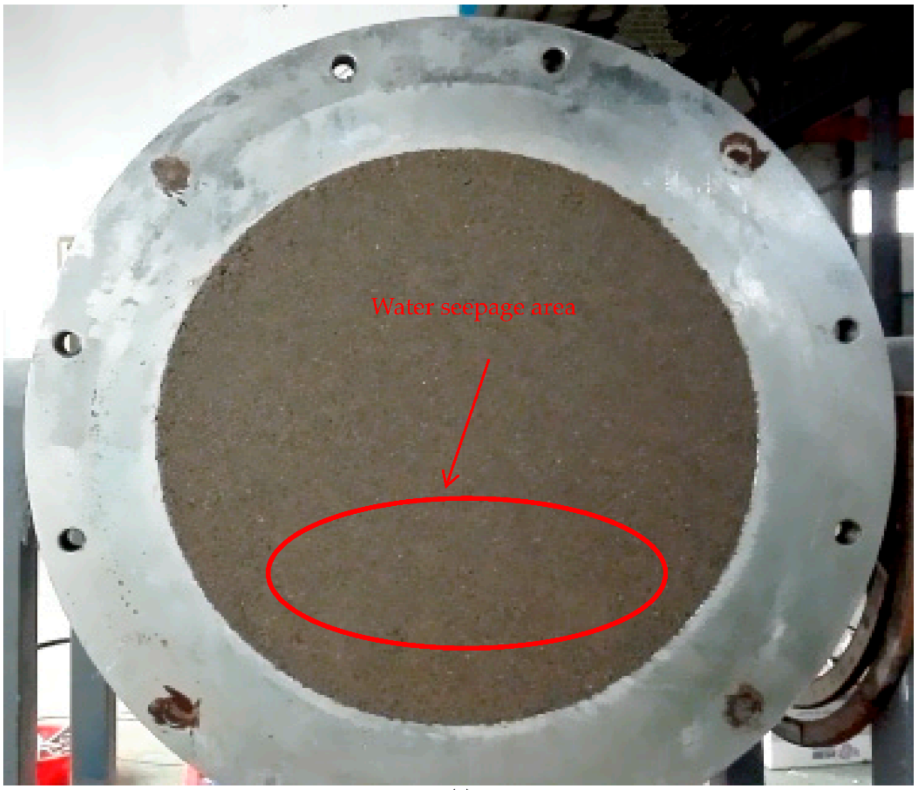

(a)

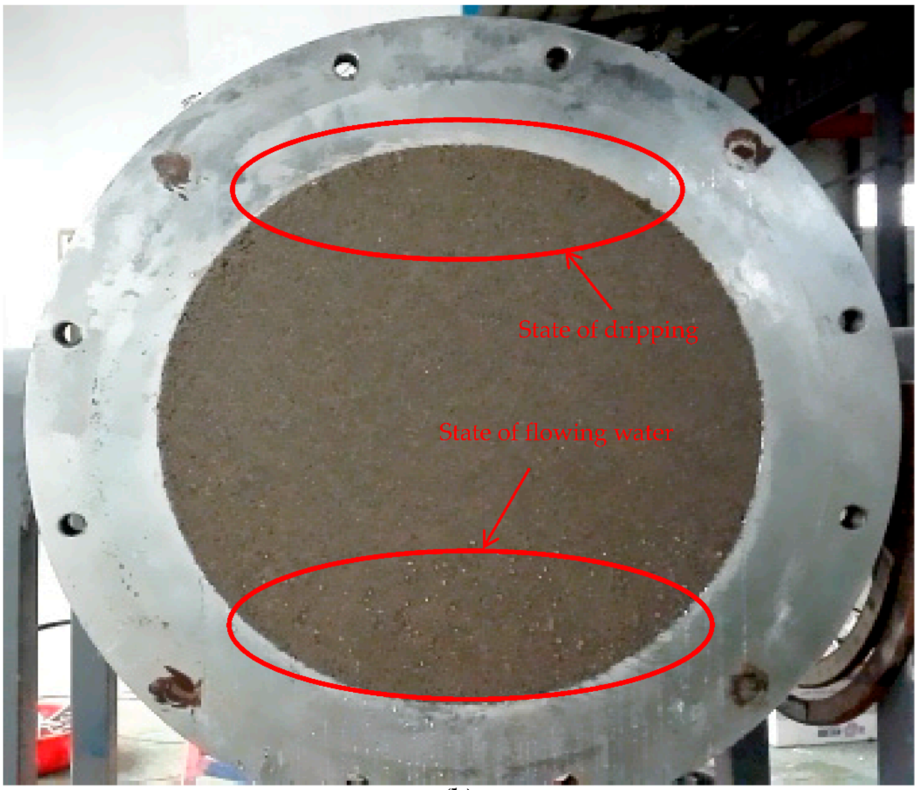

(b)

Figure 7. Water seepage stage in front of the tunnel face. (**a**) Water seepage in the lower part; (**b**) the seepage area is covered with the surface of the aquifuge rock.

Simultaneously to the rock uplifts, the crack continued extending about 20° to the upper left, and the extension speed accelerated. Then, a large crack appeared in the near vertical direction of the crack with the continuous expansion of the cracks. The aquifuge rock broke down instantaneously, and water inrush occurred. In the lower and lower right, there were small blocks of aquifuge rock bodies falling sporadically under the action of water pressure after the first phase of the aquifuge rock falling, which formed the phenomenon of the second stage of water inrush and mud gushing. As the aquifuge rock broke down, the water pressure loading system began releasing pressure, and then, the natural water supply condition occurred. The details are shown in Figure 8.

Cracks were found in the aquifuge, before the cracks expanded and extended. The first water inrush occurred in the aquifuge rock, and then, small rocks fell to form the second stage of gushing mud. The duration of the whole process was very short—less than two seconds. If it happens instantaneously, and the whole body of the aquifuge rock outbursts, then the degree of harm would be great.

During the water-inrush test, the aquifuge rock fractured and outburst holistically. Therefore, with the breaking off of the aquifuge rock, the pressure relief of the dissolved cavity was instantaneous, and water flowed out of the dissolved cavity naturally. Water inrush stopped after the pump was stopped.

(**a**)

Figure 8. *Cont.*

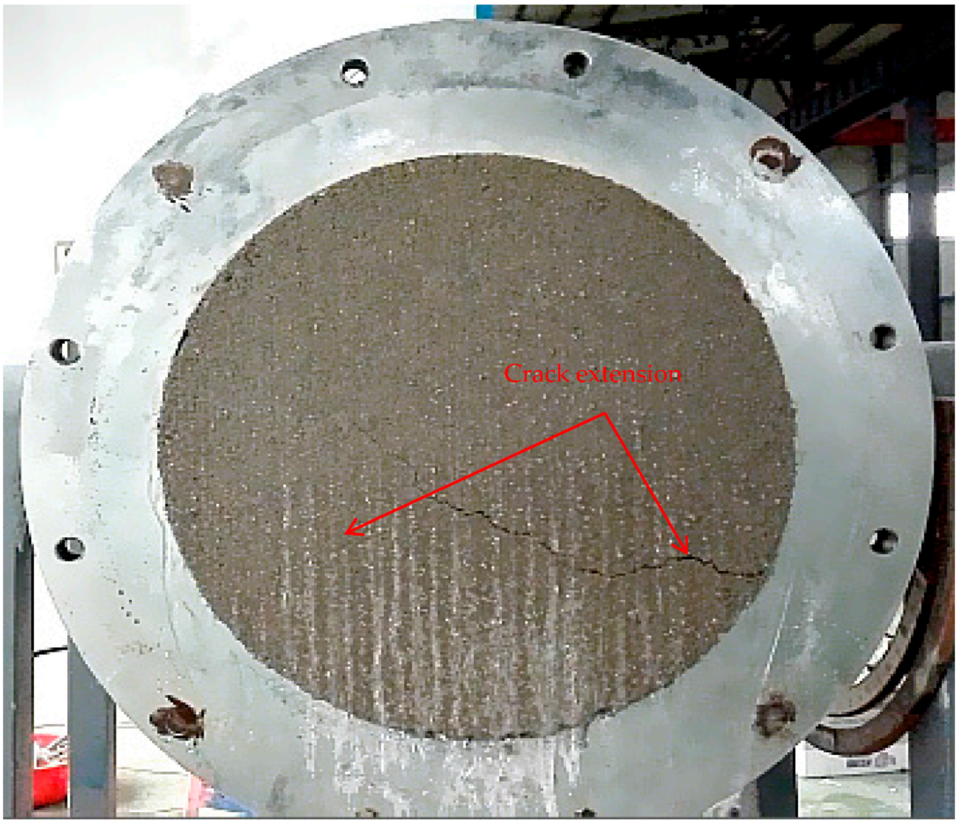

(b)

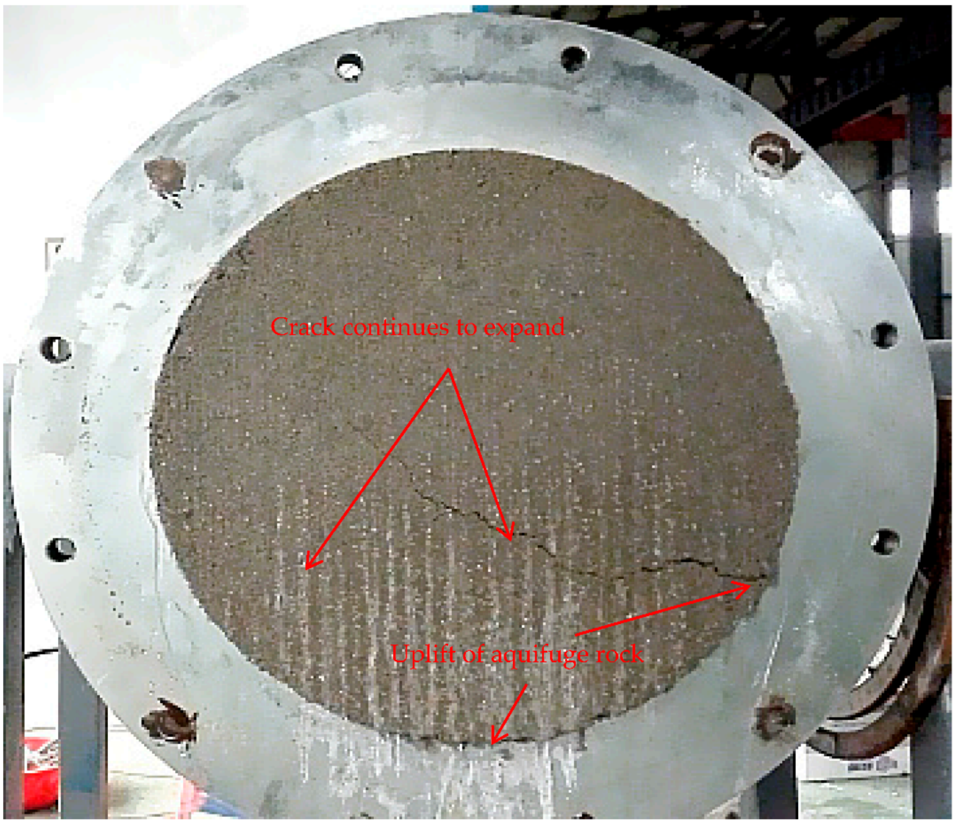

(c)

Figure 8. *Cont*.

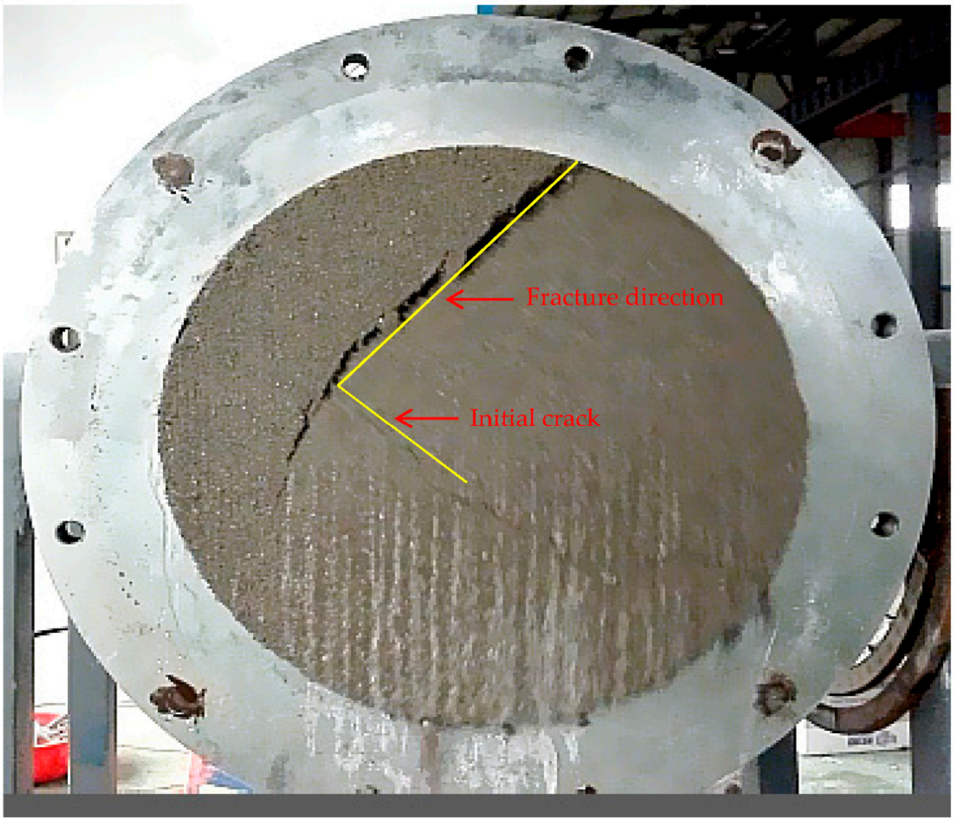

(d)

(e)

Figure 8. *Cont.*

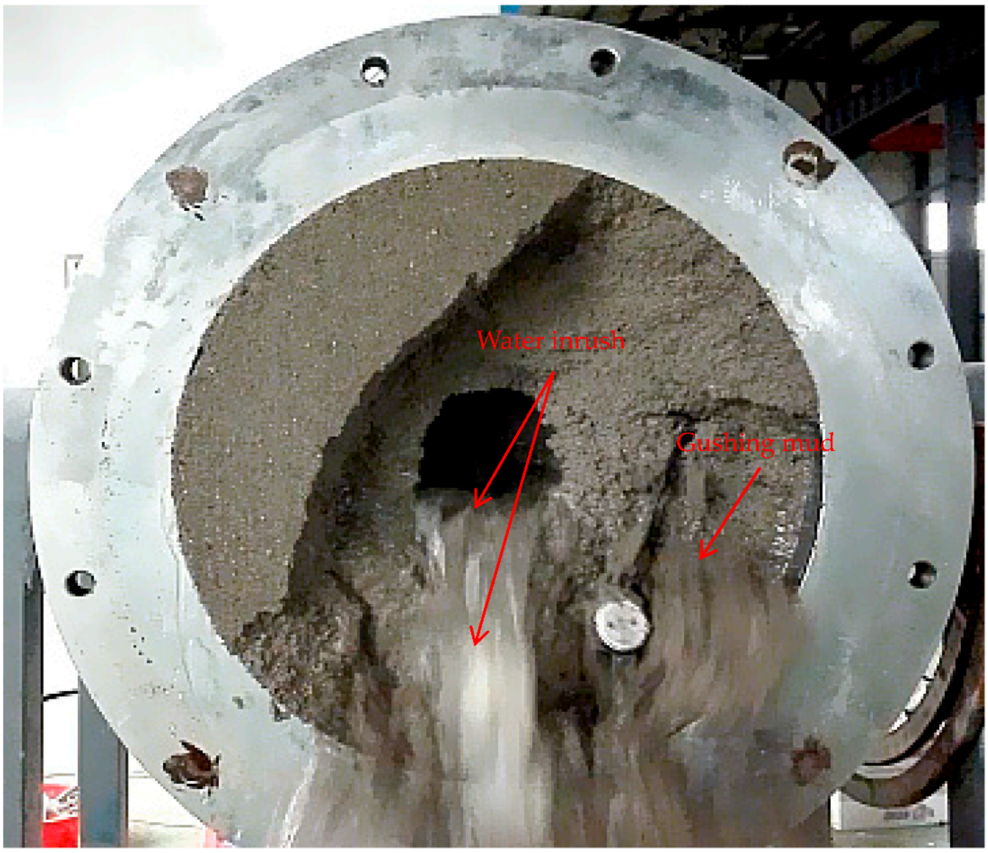

(**f**)

Figure 8. Water inrush stage at the bottom of arch. (**a**) The crack continued to extend about 20° to the upper left. (**b**) The crack extension. (**c**) Uplift of aquifuge rock. (**d**) A large crack appeared in the near vertical direction of the crack with the continuous expansion of the cracks. (**e**) The aquifuge rock broke down. (**f**) Water inrush occurred.

4.1.3. Water Inrush of Cavity at the Bottom of Arch

During the seepage stage before water inrush, when the pressure increased to 0.3 MPa, water droplets appeared only in the small area above the prefabricated dissolved cavity, and the droplets were attached to the surface of the aquifuge rock. There was no trend in flow. No abnormal phenomenon occurred in the aquifuge after retention for 10 min; thus, the water pressure was increased. When the pressure rose to about 0.35 MPa, the water seepage area increased dramatically, and there was a flow-like trend. The seepage area of the working condition was almost instantaneously filled with the whole surface of the aquifuge rock, which almost omitted the local seepage stage. This was different from the above two kinds of working conditions, as the seepage area was slowly scattered from the local to the entire surface of the aquifuge rock. The surface seepage zone of the aquifuge rock was formed into a sheet area with the increase in water pressure, and the seepage velocity increased continuously (Figure 9).

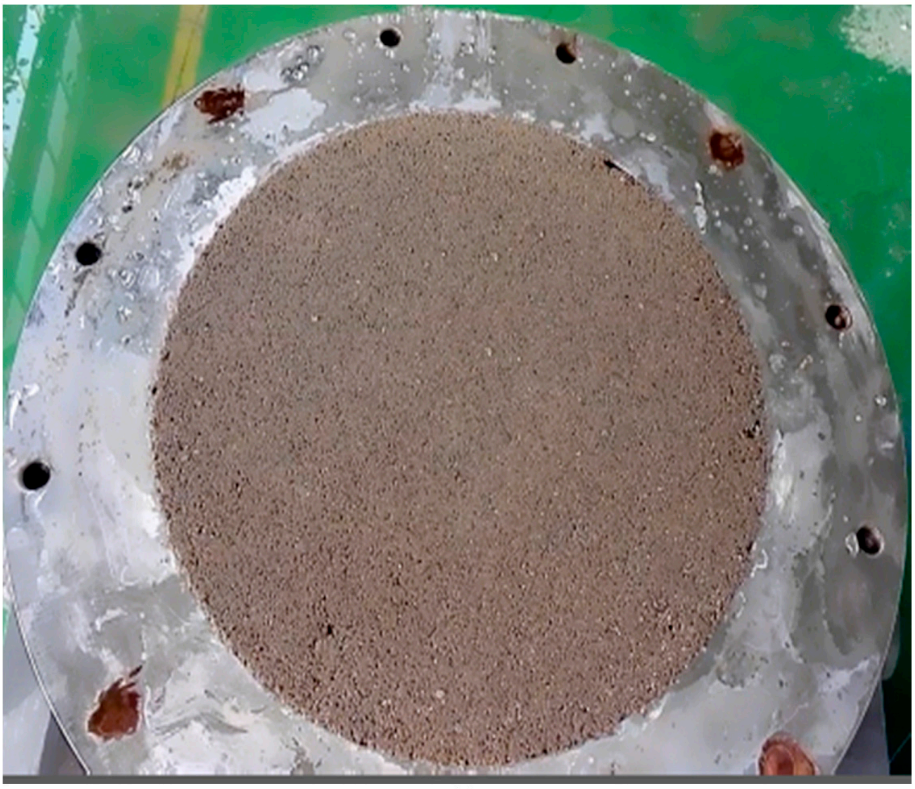

(**a**)

(**b**)

Figure 9. *Cont*.

(**c**)

(**d**)

Figure 9. Water seepage stage at the bottom of arch. (**a**) The initial state. (**b**) Local water droplet attachment. (**c**) Instantaneous expansion of seepage zone. (**d**) The water seepage area is connected into one piece.

During the water-inrush stage, the seepage velocity of the aquifuge rock accelerated continuously with increasing water pressure. A long, white bubble appeared in the middle of the aquifuge rock at hydraulic pressure loading of 0.45 MPa. This occurred as a result of the formation of surface cracks. Several cracks extended outward from the center of the aquifuge rock after a short duration of time. As the water pressure continued increasing, the cracks continued expanding and extending, forming a large fissure and several small cracks, and the bottom had a tendency to uplift. The cracks continued expanding with increasing water pressure. We clearly observed the process of small cracks expanding and merging into large cracks until two intersecting cracks formed a cross-shape. Additionally, the initial large-crack expansion degree was higher than the other three large cracks extending the extent of expansion.

In the process of hydraulic loading, a water outlet appeared at the edge of the aquifuge rock, and the whole aquifuge rock was continuously uplifted because of the continuous scour of water. When the hydraulic pressure reached 0.5 MPa, the water velocity of the edge outlet was aggravated, the uplift velocity of the riser was obviously slow, and the water spurted out from the middle of the aquifuge rock. The hydraulic loading system instantaneously released pressure because of the water inrush of the aquifuge rock, and the position of water inrush in the middle changed from a jet to gushing water. The hydraulic loading system was shut down to stop the water supply, and this was the end of water inrush. The process of water inrush is shown in Figure 10.

During the water-inrush stop stage, the inrush stopped after the water pressure loading system shut down. A stratified rupture occurred at the edge of the water inlet, resulting in the formation of a gushing water outlet and water gushing occurred. The height of the rock was measured after the remaining water in the cavity drained, and the model body stabilized. The highest uplift in the central part was about 2.3 cm. The aquifuge rock after water inrush is shown in Figure 11.

(**a**)

Figure 10. *Cont.*

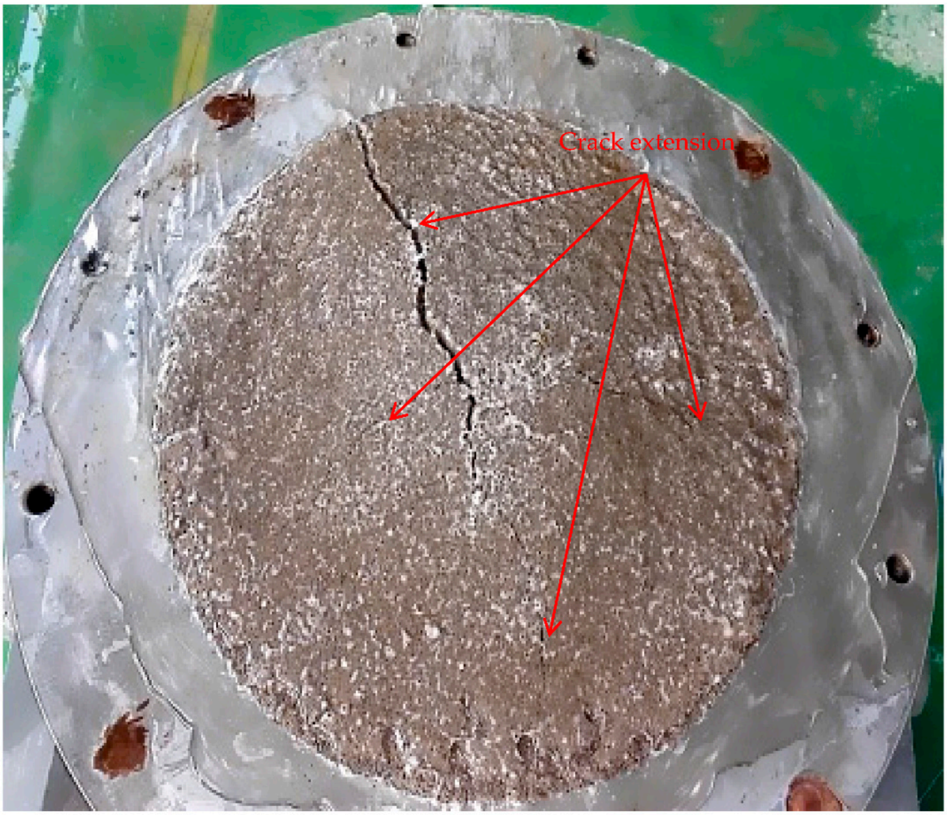

(**b**)

(**c**)

Figure 10. *Cont*.

(**d**)

Figure 10. Water inrush stage at the bottom of arch. (**a**) White bubble appeared in the middle of the aquifuge rock. (**b**) The crack extension. (**c**) Cross-shaped cross crack and uplift of aquifuge rock. (**d**) Water inrush occurred.

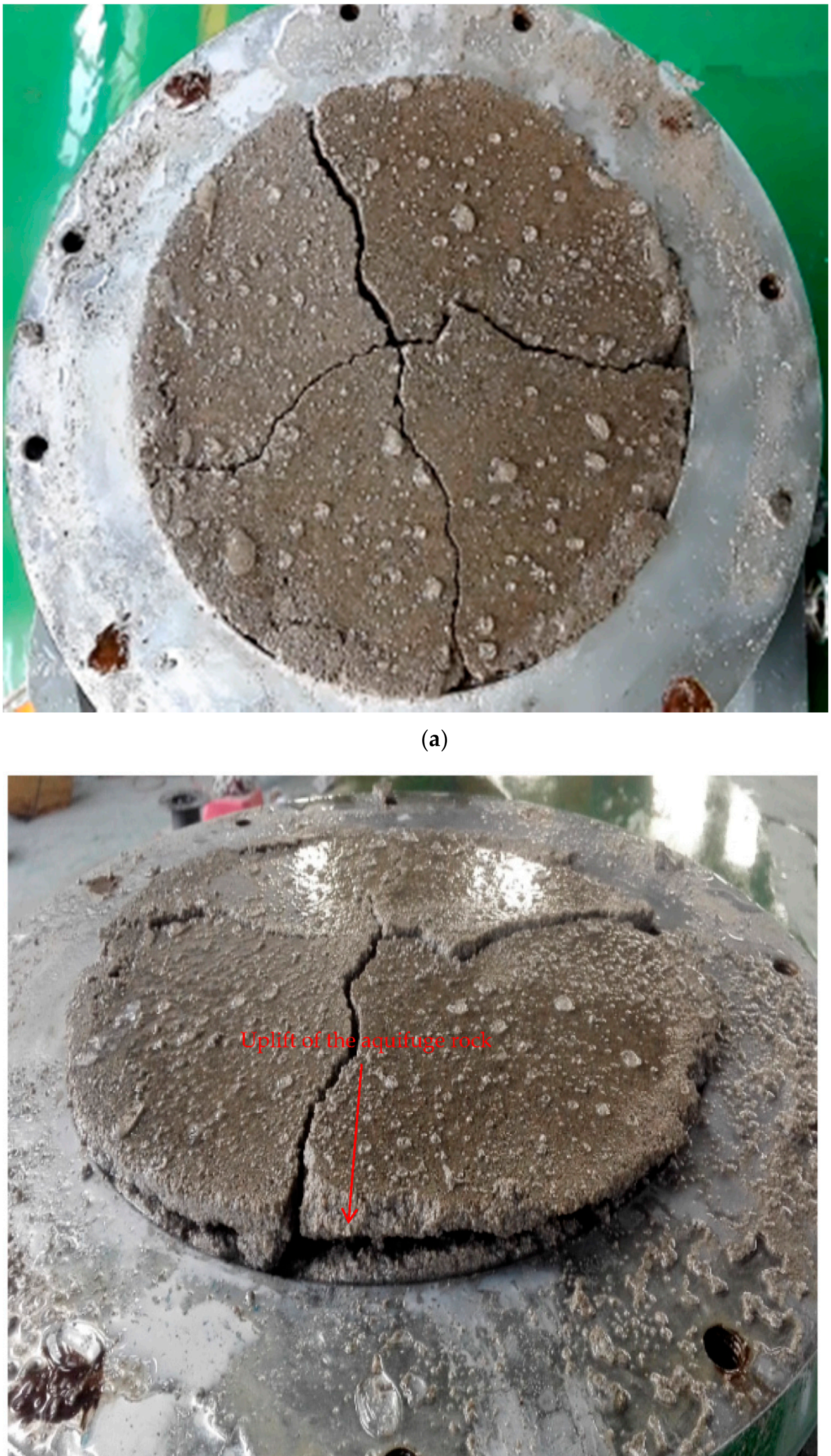

Figure 11. The picture of rock after water inrush at the bottom of arch. (**a**) The water inrush stopped after the water pressure loading system shuts down. (**b**) Uplift of the aquifuge rock.

4.2. Variation Regularity of Seepage Pressure in the Aquifuge Rock

According to the variation law of seepage pressure in aquifuge rock, the variation in the aquifuge rock in the process of water inrush in front of the tunnel face was divided into three stages, combined with the analysis of the characteristics of the aquifuge rock in the preceding test: (I) crack generation, (II) holing-through of fracture and forming of water inrush channel, and (III) water-inrush stage.

4.2.1. Water Inrush in the Vault Cavity

As shown in Figure 12, in the early stages of the experiment, the water pressure at the monitoring point of the aquifuge rock was approximately 0 before the loading pressure reached 60 kPa because of the permeability of water-resisting material. Then, the water pressure slowly rose to 25.74 kPa. It can be seen that water seepage appeared at the beginning of this stage, combined with the characteristics of the above test process, which was defined as the crack-generation stage (stage I).

The seepage pressure at the monitoring point of the aquifuge rock increased with increasing pressure loading, and the growth rate sped up. The seepage pressure of the aquifuge rock rose to 255.92 kPa at the end of stage II, and then, the seepage pressure continued increasing, but the growth rate decreased obviously. Combined with the analysis of the characteristics of the aquifuge rock, the seepage zone extended to the whole surface of the aquifuge rock, the seepage velocity intensified, and the aquifuge rock had the tendency to break water inrush. Therefore, the internal fissures of the aquifuge rock expanded with continuously increasing water pressure. Because of the increase in water pressure, the increase in seepage pressure in the third stage was obviously slower than in the second stage because the water-inrush channel formed at the end of the stage II, and stage II was defined as the fissure extension to the water-inrush channel.

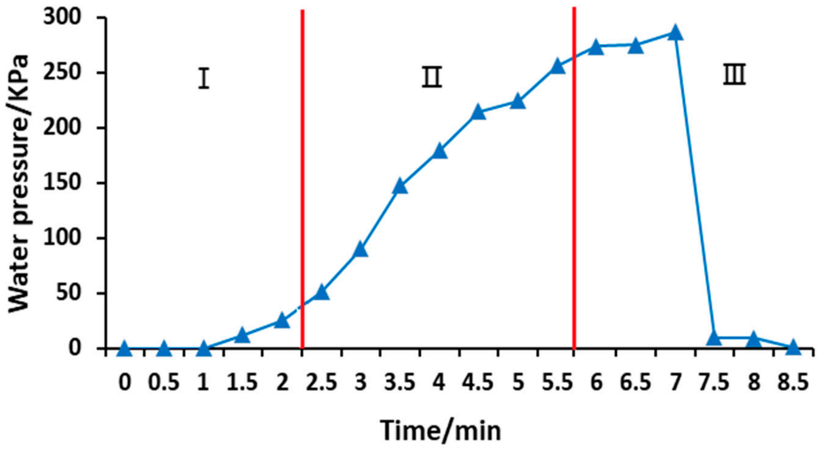

Figure 12. Water pressure variation of aquifuge rock in the process of water inrush in the vault cavity.

The seepage pressure in the monitoring point of the aquifuge rock grew slowly during the early part of stage III, and the aquifuge rock cracked and burst when the osmotic pressure increased to 286.81 kPa. As can be seen from the Figure 12, the seepage pressure of the aquifuge rock fell steeply. In the analysis of the above characteristics, we knew that the water inrush was appearing in the aquifuge rock, and the osmotic pressure decreased with falling off the block. However, the seepage pressure dropped to 0 as the seepage pressure monitoring point fell with the block body of the aquifuge rock.

4.2.2. Water Inrush of Cavity in Front of the Tunnel Face

The water pressure variation of the aquifuge rock in the process of water inrush in front of the tunnel face is shown in Figure 13. During stage I, the seepage pressure of the aquifuge rock increased slowly from 0 to 15.36 kPa and the loading water pressure reached 120 kPa. According to the analysis of the characteristics of the preceding test process, the seepage area appeared below the aquifuge rock. The seepage area spread to the top with increasing loading water pressure, and the fissures began occurring.

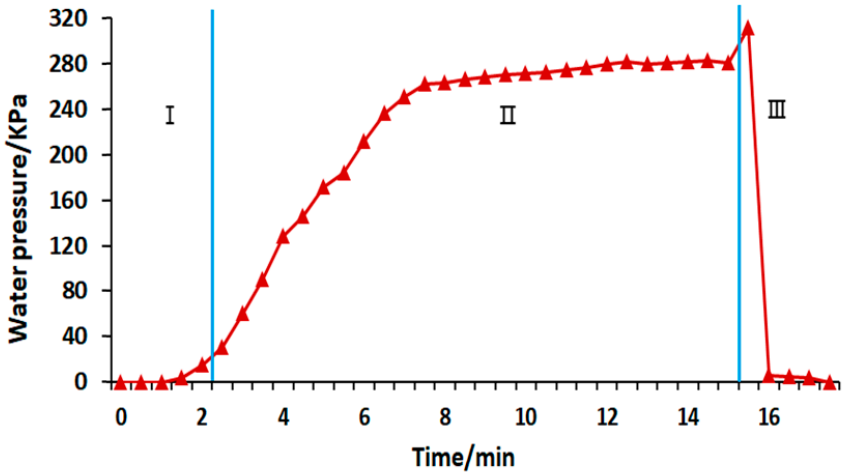

Figure 13. Water pressure variation of aquifuge rock in the process of water inrush of cavity in front of the tunnel face.

In the early part of stage II, the seepage pressure increased at the monitoring point of the aquifuge rock from 15.36 kPa to 250.71 kPa during the first seven minutes of test time, and the growth rate sped up. Because pressure was maintained for 10 min when the loading pressure reached 300 kPa, the seepage pressure at the monitoring point of the aquifuge rock slowly increased during the latter part of stage II. The seepage pressure at the monitoring point of the aquifuge rock only changed from 250.71 kPa in the middle (7 min) to 280.50 kPa at the end of stage II (15 min), that is, the monitoring point of the aquifuge rock increased by about 30 kPa eight minutes after entering the holding period. According to the analysis of the characteristics of the aquifuge rock, the seepage zone extended to the whole surface of the aquifuge rock, and the water seepage area beneath the aquifuge rock was gradually connected with the trend in the flake. The water inrush in the aquifuge rock occurred after a short period of water pressure loading at the end of the pressure-retaining period. Therefore, we believed that the water-inrush passage in the aquifuge rock formed during the period of pressure retention, and the transient water pressure increase was only a precipitating factor.

The pressure at the speed of 60k Pa/min continued loading after the pressure-retaining period was finished, and the seepage pressure at the monitoring point of the aquifuge rock increased from 280.50 kPa to 312.12 kPa. Then, the seepage pressure at the monitoring point of the aquifuge rock dropped suddenly to 6.01 kPa, and then decreased to 0. According to the analysis of the characteristics of the aquifuge rock, we knew that the seepage zone of the lower part of the aquifuge rock gradually formed flake seepage, before the aquifuge rock outburst, and water inrush occurred along with the occurrence of mud gushing in the local area.

4.2.3. Water Inrush of Cavity at the Bottom of Arch

As shown in Figure 14, during phase I in the test, the seepage pressure of the aquifuge rock increased slowly with the loading pressure before the loading pressure reached 300 kPa. Then, the test entered the retention period, keeping the loading water pressure at 300 kPa for about 10 min. The seepage pressure at the monitoring point of the aquifuge rock at this stage changed from 84.30 kPa to 95.82 kPa fluctuating. According to the analysis of the characteristics of the preceding test process, we knew that the aquifuge rock was only attached to a few drops in the upper area of the dissolved cavity and there was no large-scale seepage phenomenon. Therefore, this was defined as the phase of fracture generation.

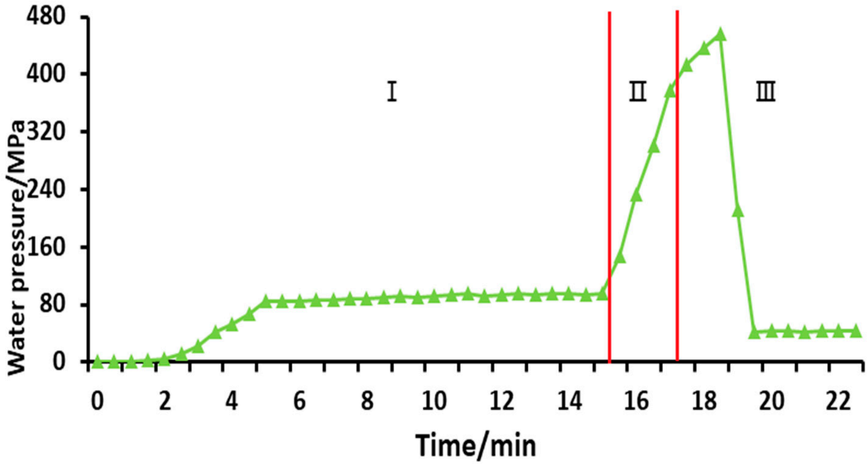

Figure 14. Water pressure variation of aquifuge rock in the process of water inrush of cavity at the bottom of arch.

The water pressure was loaded according to the established plan after the pressure-retaining period finished. The seepage pressure at the monitoring point of the aquifuge rock increased, and the increasing rate accelerated. The seepage pressure of the aquifuge rock increased from 95.82 kPa to 377.00 kPa at the end of stage II, with a growth rate of about 153.53 kPa/min. The growth rate of seepage pressure of the aquifuge rock was 44.20 kPa/min in the prophase of stage III. According to the analysis of the characteristics of the aquifuge rock, the water droplets attached at the above-dissolved cavities were instantaneously diffused to the surface of the aquifuge rock, and the surface of the aquifuge rock was characterized by a flake flowing water with a trend of overall prominence. Therefore, the stage (from 15.5 min to 17 min) was defined as crack propagation and extension, and the water-inrush channel formation stage.

The seepage pressure in the aquifuge rock increased with increasing loading water pressure, but the growth rate was slower than that of stage II. The seepage pressure fell steeply when the seepage pressure reached 456.83 kPa at the monitoring point of the aquifuge rock. However, unlike the two above working conditions, the seepage pressure fluctuated over 43.00 kPa, not down to 0, after the seepage pressure at the monitoring point of the aquifuge rock stabilized. According to the analysis of the characteristics of the aquifuge rock, fissures in the middle of the aquifuge rock were found. Then, the extension expanded to form the cross-shaped crack, and aquifuge rock uplifted. Then, the middle part produced a water outlet, while the side produced gushing water. However, the aquifuge rock was not prominent as a whole, with only about 2.3 cm uplift. So the seepage pressure was still within the aquifuge rock in the late stage of water inrush.

5. Conclusions

Through the analysis of the water pressure variation law of aquifuge rock, we revealed the evolution law of water inrush from a cavity, including the initiation of fracture in the aquifuge rock, the formation of water-inrush channels, and the rupture of the aquifuge rock.

According to the characteristics of the test process, the pressure of water inrush in the vault cavity was the lowest. The seepage area spread from the central position of the aquifuge rock (the lower part of the dissolved cavity) to the whole surface of the aquifuge rock, and the aquifuge rock broke and fell, but it did not outburst, and many water-inrush ports were produced. The pressure of karst water inrush in front of the tunnel face was slightly greater than that of the vault cavity. The seepage area was from bottom to top, and the water inrush occurred instantaneously. The falling water was accompanied by the falling of small rock and gushing mud. The maximum water pressure was required for water inrush from the arch at the bottom of the tunnel. The seepage area also spread from the central position of the aquifuge (the upper part of the dissolved cavity) to the entire surface of the aquifuge rock, but the diffusion time was very short, with instantaneous properties. The aquifuge rock continuously uplifted, forming a cross-shaped crack. The water inrush occurred in the middle, and the water gushing occurred at the edge.

By analyzing the seepage pressure changes at the monitoring points of the aquifuge rock, we divided the water-inrush process of the cave into three stages: (I) crack-generation stage, (II) holing-through of fracture and forming of water-inrush channel stage, and (III) water-inrush stage.

In this paper, the laboratory simulation of water inrush did not involve the simulation of ground stress. Therefore, in order to better simulate actual working conditions, ground stress should be considered by applying a certain ground stress to the model body by modifying the existing test system in future research.

Author Contributions: Z.Z. and H.W. conceived and designed the experiments; Z.F. performed the experiments; S.S. and L.B. analyzed the data; L.L. contributed reagents/materials/analysis tools; W.Y. and X.Y. wrote the paper; J.W. and X.L. constructed the manuscript structure in the manuscript revision.

Funding: This research was funded by National Natural Science Foundation of China (Grant No. 51479107, Grant No. 51609129), State key laboratory for Mine disaster prevention and control, cultivation base co-built by province and Ministry of Shandong University of science and technology (Grant No. MDPC201707), Shandong postdoctoral innovation project special Foundation (Grant No. 201502025), The Fundamental Research Funds of Shandong University (Grant No. 2018JC048), National Natural Science Foundation of China (Grant No.: 51809158), Shandong Provincial Natural Science Foundation, China (Grant No. ZR2018BEE045), and China Postdoctoral Science Foundation (2018M630780).

Conflicts of Interest: The authors declare no conflicts of interest.

References

1. Liu, Z.J.; Huang, Y.; Zhou, D.; Ge, H. Analysis of External Water Pressure for a Tunnel in Fractured Rocks. *Geofluids* **2017**. [CrossRef]
2. Ma, D.; Miao, X.X.; Chen, Z.Q.; Mao, X.B. Erratum to: Experimental investigation of seepage properties of fractured rocks under different confining pressures. *Rock Mech. Rock Eng.* **2015**, *48*, 2183. [CrossRef]
3. Deng, X.H.; Yuan, D.Y.; Yang, D.S.; Zhang, C.S. Back Analysis of Geomechanical Parameters of Rock Masses Based on Seepage-Stress Coupled Analysis. *Math. Probl. Eng.* **2017**. [CrossRef]
4. Liu, Q.; Wei, L.; Chen, J.; Luo, Y.; Huang, P.; Wang, H.; Guo, J. Stability Analysis of Water-Resistant Strata in Karst Tunnel Based on Releasable Elastic Strain Energy. *Math. Probl. Eng.* **2017**. [CrossRef]
5. Hao, Y.Q.; Rong, X.L.; Ma, L.J.; Fan, P.X.; Lu, H. Uncertainty Analysis on Risk Assessment of Water Inrush in Karst Tunnels. *Math. Probl. Eng.* **2016**. [CrossRef]
6. Wei, W.W.; Chen, D.Z.; Qing, H.R.; Qian, Y.X. Hydrothermal Dissolution of Deeply Buried Cambrian Dolomite Rocks and Porosity Generation: Integrated with Geological Studies and Reactive Transport Modeling in the Tarim Basin, China. *Geofluids* **2017**. [CrossRef]
7. Xiao, M.; Zhao, C. Stability Analysis of Steel Lining at Pressure Diversion Tunnel Collapse Zone during Operating Period. *Math. Probl. Eng.* **2017**. [CrossRef]
8. Ahn, C.; Hu, J.W. Experimental Field Tests and Finite Element Analyses for Rock Cracking Using the Expansion of Vermiculite Materials. *Adv. Mater. Sci. Eng.* **2016**. [CrossRef]
9. Zhang, L.L.; Xia, L.; Yu, Q.C. Determining the REV for Fracture Rock Mass Based on Seepage Theory. *Geofluids* **2017**. [CrossRef]
10. Sterpi, D.; Cividini, A. A physical and numerical investigation on the stability of shallow tunnels in strain softening media. *Rock Mech. Rock Eng.* **2004**, *37*, 277–298. [CrossRef]
11. Li, S.C.; Liu, H.L.; Li, L.P.; Zhang, Q.Q.; Wang, K.; Wang, K. Large scale three-dimensional seepage analysis model test and numerical simulation research on undersea tunnel. *Appl. Ocean Res.* **2014**, *59*, 510–520. [CrossRef]
12. Liang, D.X.; Jiang, Z.Q.; Zhu, S.Y.; Sun, Q.; Qian, Z.W. Experimental research on water inrush in tunnel construction. *Nat. Hazards* **2016**, *81*, 467–480. [CrossRef]
13. Jiang, H.M.; Li, L.; Rong, X.L.; Wang, M.Y.; Xia, Y.P.; Zhang, Z.C. Model test to investigate waterproof-resistant slab minimum safety thickness for water inrush geohazards. *Tunn. Undergr. Space Technol.* **2017**, *62*, 35–42. [CrossRef]

14. Wang, K.Z.; Li, Z.K. Study on 3D physical model test of seepage of deep-buried long and large diversion tunnel. *Chin. J. Rock Mech. Eng.* **2009**, *28*, 725–731.
15. Pang, Y.H.; Wang, G.F.; Ding, Z.W. Mechanical model of water inrush from coal seam floor based on triaxial seepage experiments. *Int. J. Coal Sci. Technol.* **2014**, *1*, 428–433. [CrossRef]
16. Zhang, S.; Guo, W.; Li, Y.; Sun, W.; Yin, D. Experimental Simulation of Fault Water Inrush Channel Evolution in a Coal Mine Floor. *Mine Water Environ.* **2017**, *36*, 443–451. [CrossRef]
17. Li, S.C.; Zhang, Q.S. *Tunnel and Underground Engineering Water Burst Mechanism and Governance*; China Communications Press: Beijing, China, 2014; ISBN 978-7-114-11146-4.
18. Shi, S.S. Study on Seepage Failure Mechanism and Risk Control of Water Inrush Induced by Filled Disaster Structure in Deep-Long Tunnel and Engineering Application. Ph.D. Thesis, Shandong University, Jinan, China, 2014.
19. Li, S.C.; Yuan, Y.C.; Li, L.P. Water inrush mechanism and minimum safe thickness of rock wall of karst tunnel face under blast excavation. *Chin. J. Geotech. Eng.* **2015**, *37*, 313–320.